Theor Chem Acc (2007) 117:673–683
DOI 10.1007/s00214-006-0230-1

REGULAR ARTICLE

Theoretical modeling of the benzoic acid adsorption on the GaAs (001)-$\beta_2(2 \times 4)$ oxidized surface

Maria Francesca Iozzi · Maurizio Cossi

Received: 30 May 2006 / Accepted: 13 October 2006 / Published online: 26 January 2007

Abstract We describe a computational model of benzoic acid adsorbed on the most abundant and technologically important GaAs surface. The performances of many electronic devices based on organic layers deposited on semiconductor surfaces, critically depend on the quality of the layer, and thus on the features of the organic/inorganic bonds. Since very few is known about the atomic structure of such interfaces, theoretical modeling plays a central role in understanding these systems at the microscopic scale. We have optimized the structures of several clusters mimicking the unoxidized and oxidized GaAs (001) surface, using them to study the preferred arrangements of adsorbed benzoic acid molecules. The largest clusters were also used to investigate the cooperative effects between two adsorbed molecules, obtaining the most likely structure for a perfectly packed layer. Finally, we show the correlation of a microscopic observable, namely the energy of the lowest lying empty orbital concentrated on the organic moiety, with the electron affinity measured for para-substituted benzoic acids adsorbed on GaAs.

1 Introduction

It is widely recognized that the physical and chemical activity of metals and semiconductors can be greatly enhanced by the solid surface functionalization with suitable organic layers [1–8]. A number of applications have been described in the recent years, ranging from improved catalysts (with impressive gains in efficiency and selectivity), to optoelectronic devices, to new chemical and biochemical sensors with enhanced sensitivity and selectivity [9–17]. In all these cases, the design and the interpretation of the modified surface properties require a reliable modeling of the organic layer structure and of the molecule–surface binding at the atomic scale. Very useful information can be obtained by experimental techniques like AFM and STM microscopies, and angle resolved X-ray spectroscopy [18–21]: on the other hand, theoretical modeling can be extremely useful to support and complement the experimental data.

In this paper we consider the adsorption of benzoic acid on the GaAs (001) surface [12,22–24]: this surface is encountered in many applications, mainly for the fabrication of sensors [25] and optoelectronic devices [11,26], and in many cases self-assembled monolayers of organic molecules have been used to improve its performances [27–30]. The GaAs (001) surface can undergo different reconstructions, whose relative energies have been long debated [31–41]: As-rich surfaces are usually grown under conditions leading to a (2×4) reconstruction [35–39] (i.e. with a two-dimensional periodic structure whose unit cell is two times the bulk lattice distance in one direction and four times in the other). Among the possible (2×4) structures, recent calculations and accurate scanning tunneling microscopy (STM) experiments indicate the so-called $\beta_2(2 \times 4)$ as the most likely in usual conditions [36,37]: this structure is sketched in Fig. 1. Throughout this article we will always refer to this surface: as can be seen in the schematic picture, the uppermost layer is formed by arsenic dimer pairs,

M. F. Iozzi
Dipartimento di Chimica, Università di Napoli Federico II, Complesso Monte S. Angelo, via Cintia, 80126 Naples, Italy

M. Cossi (✉)
Facoltà di Scienze Matematiche Fisiche e Naturali, Università del Piemonte Orientale "Amedeo Avogadro", via Bellini 25/G, 15100 Alessandria, Italy
e-mail: maurizio.cossi@unina.it

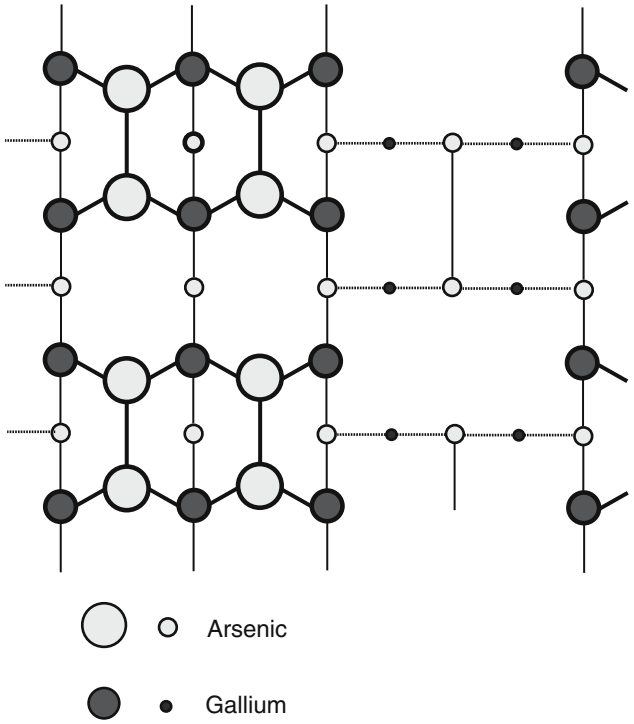

Fig. 1 Schematic picture of the GaAs(001)-$\beta_2(2 \times 4)$ surface

arranged in parallel rows, which are separated by quite deep trenches. Below each arsenic dimer pair, six gallium atoms form the base of these protruding "platforms": four of the gallium atoms have unsaturated valences (dangling bonds); other arsenic dimers are formed on the bottom of the trenches. Some experimental (STM) results [42–46] indicate that in the oxidized surface the top oxide layer is formed by Ga_2O_3, resulting from the displacement of metallic arsenic [47]: as a result, in the ideal oxidized surface the top arsenic dimer pairs should be substituted by oxygen atoms.

Benzoic and aliphatic carboxylic acid layers have been used to enhance the wettability of oxidized GaAs surfaces by liquid crystals in the preparation of 2D photonic crystals [22]; benzoic and hydroxamyc acid derivatives with varying dipole moments have been used to tune the surface work function and hence the performance of GaAs [27–30] and CdTe [17,51,52] photovoltaic cells. A very useful observable related to the electrical properties of the modified surfaces is the work function change induced by the organic monolayer. Such a change is measured as a function of the current/potential curves of semiconductor/molecular layer/metal junctions, and it is found to depend strongly on the chemical nature of the organic molecule substituents. Homologue series of benzoic acid derivatives [23], as well as of other carboxylic acid derivatives [11,28], have been used to fine-tune the work function of GaAs surfaces.

In the present paper, we consider the different possible adsorption sites of benzoic acid on this surface: very few is known about this point, except for some FTIR results suggesting a bridging coordination to Cd on CdTe [51], and a bridging or unidentate coordination to Ga on GaAs [23]; clearly a deeper understanding of the binding preference is of great importance for any model of the organic layers. When possible, we shall compare our computed vibrational frequencies to the FTIR spectra; in addition, the cooperative effects associated to the adsorption of more than one molecule in neighboring sites will be evaluated on a large cluster modeling the oxidized surface.

Finally, following an approach already applied to tartaric acid derivatives adsorbed on GaAs surfaces [53], we will test the correlation of a microscopic property (i.e. the molecular orbital energies) with the observed changes in the work function of derivatized surfaces.

2 Computational methods

DFT calculations have been performed with the Gaussian03 package [48], using the PBE1PBE density functional (also called PBE0 in some older applications): it is a generalized gradient approximation (GGA) functional, based on the Perdew, Burke and Ernzerhof functional (PBE) [49], and modified as reported in reference [50], which has proved very reliable for the calculation of organic molecule electronic properties [54–56]. This is a hybrid functional, because a part of the exchange energy is computed with the Hartree–Fock (HF) exchange Hamiltonian: the amount of the HF contribution was derived from fundamental physical constraints [50].

The Pople 6-31G [57] basis set has been employed on second row elements, supplemented in some cases by extra polarization functions on hydrogen and heavy atoms [58], and by diffuse functions on heavy atoms [59] (the resulting set being indicated as usual as 6-31+G(d,p)). On gallium and arsenic atoms the LANL2DZ set of pseudopotentials and basis [60–62] has been used; in some calculations, the Ga atoms close to the surface have been assigned an enlarged set, referred to as LANL2DZ(d), including *d* polarization functions with exponent 0.451.

Semiempirical calculations have been performed with the MSINDO method (MSINDO package, version 2.6.3 by K. Jug, T. Bredow and G. Geudtner) [63,64], based on the previous SINDO1 approach [65] with significant improvements in the basis sets and parameterization.

MSINDO has been recently extended to third row elements with an efficient parameterization [66,67] that has provided very satisfying results for structures, relative energies and dipole moments, and it is probably the best compromise presently available for the study of very large GaAs clusters.

Multi-layer calculations exploited the ONIOM scheme [68,69,76–81]: two theoretical methods, with different accuracies and computational costs, are used and a small portion of the system of interest is selected as the more important (for instance, in most of the following calculations the "small" system is formed by the top As, the underlying Ga and some of the atoms in the lower layers). Every calculation is repeated three times: first the real system is studied at low level, and the set of relevant observables $\{O_{\text{low}}^{\text{real}}\}$ (e.g. energies, dipole moments, nuclear gradients) are computed and stored; then the small system is treated both at low and high levels, and $\{O_{\text{low}}^{\text{small}}\}$ and $\{O_{\text{high}}^{\text{small}}\}$ are computed. The final observable values are defined as

$$O_{\text{ONIOM}} = O_{\text{low}}^{\text{real}} - O_{\text{low}}^{\text{small}} + O_{\text{high}}^{\text{small}} \quad (1)$$

In the present work, the high and low level procedures are DFT and MSINDO, respectively: the Gaussian03 package was modified by the authors to allow the interface to MSINDO as an "external" program. This approach can be used very efficiently for geometry optimizations of large adducts, obtaining a good description of the chemical bonds at the interface and including (even if at a lower level) the effect of the underlying inorganic layers; note that the same scheme could also be extended to more than two levels. A delicate point is the description of the small system boundary: if, as usual, the high-level portion is defined by cutting some of the real system covalent bonds, it is necessary to saturate its valences (to avoid spurious distortions of the electron density). In the present work we adopted the standard approach of substituting the disappeared real atoms with hydrogens (scaling the bond distance by a factor of 0.8); other recipes have also been proposed [70–73], mainly for organic/biochemical applications.

3 Surface models

3.1 Unoxidized surface

The GaAs surface was modeled with two clusters of different sizes: the smaller is the $Ga_{20}As_{20}H_{32}$ cluster [74] shown in Fig. 2: it is an 8-layer cluster, where all the edge atoms are terminated with hydrogens, except those of the two first layers from top (the "surface atoms").

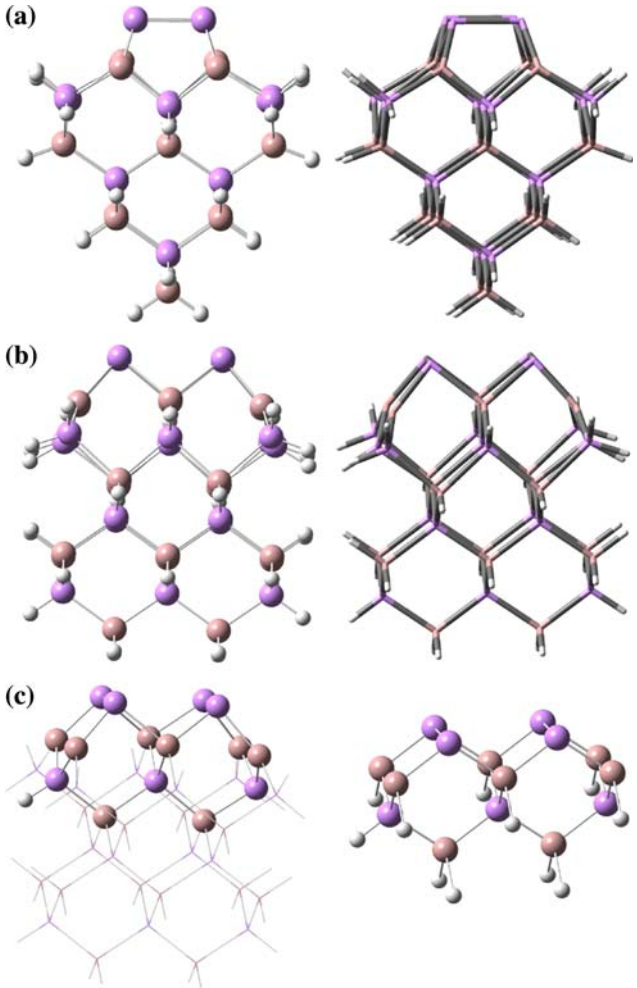

Fig. 2 $Ga_{20}As_{20}H_{32}$ cluster: **a**, **b** side views; **c** cluster portion treated at DFT level in ONIOM calculations, without and with the H atoms added to saturate the valences

This cluster models one of the protruding platforms observed on the GaAs surface: the uppermost layer is formed by two As dimers, followed by six Ga atoms, partially unsaturated.

The structure of the cluster was optimized both at DFT and ONIOM levels, to test the performances of the hybrid approach on this relatively small system. In the ONIOM calculations the DFT level was concentrated on the surface atoms (see Fig. 2c), adding hydrogen atoms to replace the As atoms cut in the definition of the small system. The initial cluster geometry was obtained from the crystallographic GaAs bulk structure [75]: during all the optimizations, the positions of all the atoms in the first five layers from bottom were frozen in their bulk values. The most relevant geometrical parameters are listed in Table 1: refer to Fig. 3 for the definition of the parameters (the complete sets of the optimized

Table 1 Most relevant geometrical parameters (Å) for the $Ga_{20}As_{20}H_{32}$ cluster optimized at DFT and ONIOM levels (see Fig. 3 for parameter definition)

	DFT	ONIOM
$dy_{1,1'}$	2.63	2.64
$dy_{3,3'}$	3.72	3.85
$dy_{4,4'}$	3.62	3.81
$dx_{1,2}$	3.98	4.15
$dz_{1,3}$	1.62	1.61
$dz_{3,4}$	0.18	0.25
$dz_{1,5}$	3.08	3.12

Table 2 Most relevant geometrical parameters (Å) for the$Ga_{20}As_{16}O_4H_{32}$ cluster optimized at DFT and ONIOM levels (see Fig. 3 for parameter definition)

	DFT	ONIOM
$dy_{1,1'}$	4.52	4.11
$dy_{3,3'}$	4.24	3.94
$dy_{4,4'}$	4.29	3.91
$dx_{1,2}$	3.24	3.55
$dz_{1,3}$	0.78	0.82
$dz_{1,5}$	1.84	2.11

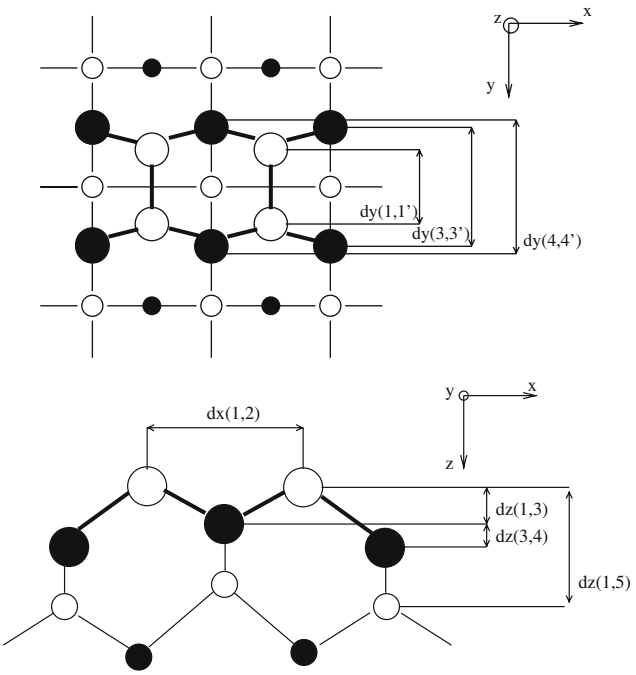

Fig. 3 Definition of the most relevant geometrical parameters on the reconstructed GaAs surface

coordinates are available on request; in the bulk structure all the Ga–As bond distances are 2.46 Å).

The ONIOM procedure proves to be reliable in the description of the surface structure. The As dimer geometry is very similar to that of the full quantum calculation, and also the distance between the dimers and the underlying Ga atoms is fairly well reproduced, the main difference being that the Ga layer is slightly wider when optimized by ONIOM (see $dy_{3,3'}$ and $dy_{4,4'}$ in Table 1).

The larger model, displaying more surface features and useful for the successive study of cooperative effects in the organic layer, is the $Ga_{108}As_{109}H_{109}$ cluster presented in Fig. 4: it comprises two adjacent rows of "platforms" (containing several As dimers), separated by a trench with three As dimers on the bottom.

To lower the computational burden, this cluster is thinner, including only six layers, and it is no longer stoichiometric: the structure of the surface, however, is still correct. The structure in Fig. 4 has been optimized at the MSINDO level, freezing the three bottom layers at their bulk positions: note that the misalignment between top and trench dimers is due to the crystalline structure and clearly visible in STM images. An important parameter for the adsorption processes is the size of the trench: in our MSINDO optimization, the trench is about 12 Åwide between the parallel As dimer rows, and 8.9 Å considering the underlying Ga atoms (w_1 and w_2 in Fig. 4, respectively); its depth is about 5.5 Åfrom the As dimers and about 3 Åfrom the Ga (d_1 and d_2 in Fig. 4).

3.2 Oxidized surface

As mentioned in Sect. 1, STM evidences indicate that the preferred oxidation sites are the "platforms" carrying the As dimer pairs, that are displaced by the oxygen atoms to eventually form metallic arsenic grains [44–47].

The oxidized surface has been modeled using the same clusters described earlier, substituting the As atoms on the platform top with oxygens: the resulting $Ga_{20}As_{16}O_4H_{32}$ and $Ga_{108}As_{85}O_{24}H_{109}$ clusters are shown in Figs. 5 and 6.

As before, the smaller cluster was optimized at DFT and ONIOM levels, freezing the first five layers from bottom, whereas the large one was optimized with MSINDO: the relevant parameters for $Ga_{20}As_{16}O_4H_{32}$ are listed in Table 2. In this case the ONIOM performance is less satisfactory than for the unoxidized cluster, so that in the following we resorted to full quantum calculations for the benzoic adducts on the small cluster; on the other hand, the ONIOM results are acceptable for the adducts on the large cluster, that would not be affordable at the higher level.

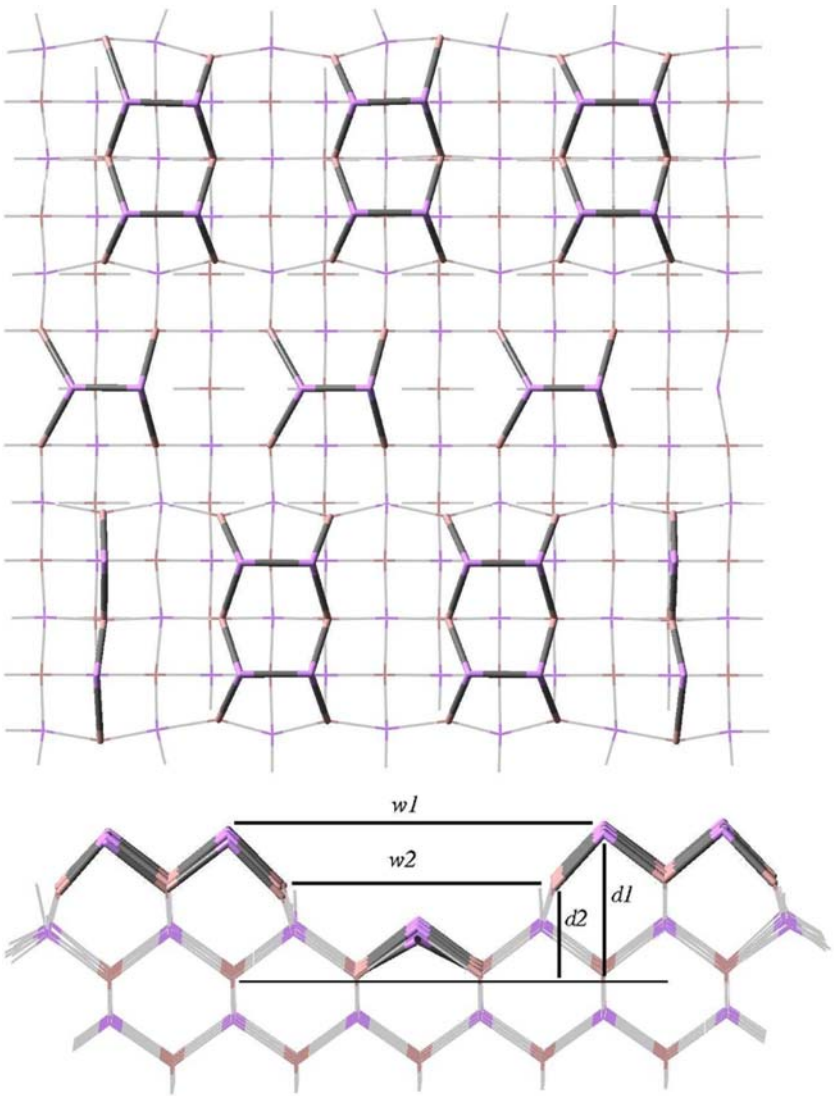

Fig. 4 $Ga_{108}As_{109}H_{109}$ cluster optimized at MSINDO level

4 Adsorption sites

Our first goal is to determine the preferred adsorption sites for benzoic acid on an oxidized platform, using the $Ga_{20}As_{16}O_4H_{32}$ cluster previously optimized (Fig. 5). It is commonly assumed that the oxidized surface is more basic than the benzoic carboxylate, so that the first step is the protonation of one of the surface oxygens: actually, in all the adduct geometry optimizations described later, even when starting from undissociated acid, the carboxylic hydrogen left the organic molecule to protonate the surface.

The benzoate can bind to the Ga atoms through monodentate (M), bidentate chelating (BC) or bidentate bridging (BB) modes (Fig. 7): considering that six gallium atoms are available, and that one of the oxygens has been protonated, there are eight possible adduct arrangements, as depicted in Fig. 8.

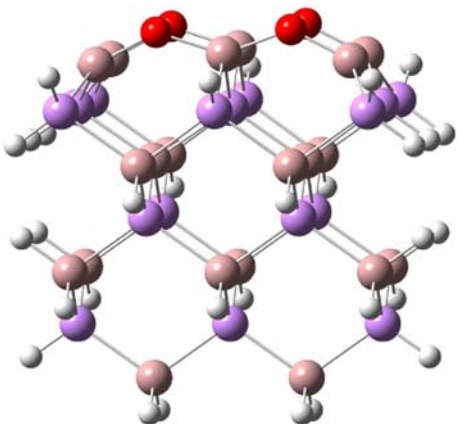

Fig. 5 Small model of the oxidized GaAs cluster: $Ga_{20}As_{16}O_4H_{32}$

To avoid pentavalent Ga's, the carboxylate should bind to the "external" atoms (1, 2 or 5, 6), which carry

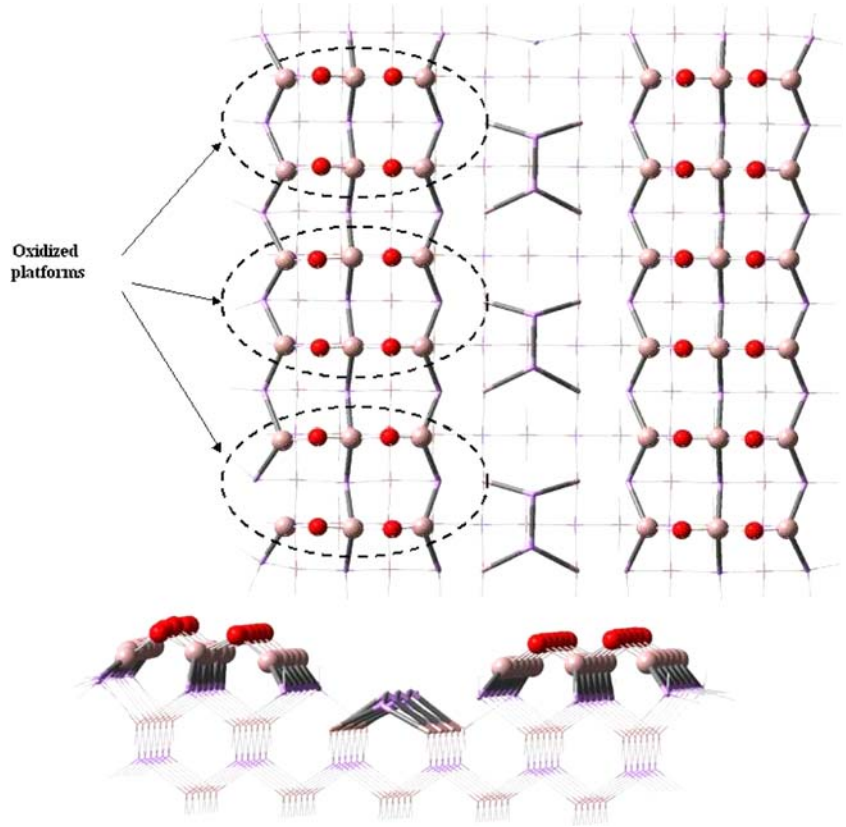

Fig. 6 Large model of the oxidized GaAs cluster: $Ga_{108}As_{85}O_{24}H_{109}$

monodentate (M)	bidentate chelating (BC)	bidentate bridging (BB)

Fig. 7 Binding modes for benzoate on Ga atoms

1,2-BB	5,6-BB
3,4-BB	3,5-BB
3-M	5-M
6-M	5-BC

Fig. 8 Possible arrangements for benzoate adsorbed on the protonated surface

empty orbitals (dangling bonds) suitable for the nucleophilic attack: the 3,4-BB adduct was included since the protonated oxygen can easily leave the Ga(3) restoring a proper coordination, at least on this side of the bridge. For the same reason, the only BC mode involves the Ga(5); M modes on Ga(1) and (2) can be considered similar to that on Ga(6): moreover, we shall see in the following that the preferred binding sites concentrate around the protonated oxygen, which "activates" the neighboring Ga atoms by weakening the Ga–O bonds.

The first screening was performed by optimizing the geometry of the eight adducts at the ONIOM (PBE1PBE:MSINDO) level, and then computing the adsorption energy, $E_{ads} = E_{adduct} - E_{cluster-H^+} - E_{benzoate}$, as single-point calculations at the PBE1PBE level. In all the DFT calculations, the 6-31G basis set was used on first and second row atoms, while the LANL2DZ set of pseudopotentials and corresponding basis set were used on As and Ga. In the ONIOM procedure, the high-level layer comprised the organic moiety, the four surface oxygens and the six underlying gallium atoms. Four structures (see Fig. 8) resulted most stable, namely 5,6-BB, 3,4-BB, 3,5-BB and 5-BC, that was actually indistinguishable from 5-M: one can see that the nucleophilic attacks take place preferably around the protonated oxygen. Interestingly, we could not find a stable minimum for 1,2-BB, since the surface OH group attracted the benzoate towards the other side of the platform, ending up with the 5,6-BB structure.

In the second step the selected structures were reoptimized at the PBE1PBE level (then extending the high-level calculation to the whole adduct), and E_{ads} was computed at the same level: this led to exclude the 3,4-BB structure also. Finally, the last three adducts were optimized, and E_{ads} was computed with a larger basis set, namely 6-31G(d,p), with the results reported in

Table 3 Relative adsorption energies (kcal/mol) and carboxylate stretching harmonic frequencies (cm^{-1}), computed at the PBE1PBE/6-31G(d,p) level for the three most stable adducts

Ads. mode	E_{ads}	ν_{asymm}	ν_{symm}	$\Delta\nu$	Exp. $\Delta\nu$ [23]
5,6-BB	0.0	1,593	1,450	143	
5-BC	8.0	1,638	1,500	138	135
3,5-BB	38.0	1,605	1,491	114	

Table 3. Two adduct structures are clearly favored, namely 5,6-BB and 5-BC: they are on the same side as the protonated oxygen, as expected, and their relative energy is small enough to allow the presence of both, although the former is more likely; all the other structures have energies far too high to be plausible.

This result can be checked by computing the vibrational frequencies associated with the carboxylate group, which are expected to be quite sensitive to the binding mode: the most relevant parameter is the splitting between the symmetric and antisymmetric stretching modes, $\Delta\nu_{str}$, which is related to the amount of charge delocalization between the oxygens. In Table 3 we report the harmonic frequencies computed for the carboxylate stretchings in the three adducts, along with the experimental $\Delta\nu_{str}$ measured by Bastide et al. [23] for a monolayer of benzoic acid on GaAs. One can see that the experimental evidence agrees with 5,6-BB or 5-BC binding, confirming the E_{ads} trend. Note that the same authors report a $\Delta\nu_{str}$ of 144 cm^{-1} for the free carboxylate (i.e. when the two oxygens are perfectly equivalent): both the computed and the measured frequency splitting indicate that in the adduct this equivalence is preserved fairly well.

5 Cooperative effects

Having determined the preferred adsorption sites for a single molecule, we have investigated the structure of highly packed organic layers. A preliminary information can be obtained by computing the interaction energy of two benzoic acid molecules in different orientations: the isolated molecule geometry was optimized at the PBE1PBE/6-31G level, then the dimer energy was scanned with respect to the intermolecular distance, without reoptimizing the two fragments, in the three arrangements shown in Fig. 9. The resulting curves are reported in Fig. 10: in the side-to-face orientation a minimum exists at 5.3 Å, with a small stabilizing energy of about −1 kcal/mol with respect to the two isolated fragments; on the other hand, the side-to-side and face-to-face arrangements produce repulsive curves at all distances.

Table 4 Relative adsorption energy (kcal/mol) for one and two benzoic acid molecules on the $Ga_{108}As_{85}O_{24}H_{109}$ cluster: see Fig. 12 for the various arrangements

Adduct structure	E_{ads} per adsorbed molecule
One molecule (BB mode)	0.0
One molecule (BC mode)	0.5
Two molecules (a)	+7.5 (+2.0[a])
Two molecules (b)	+2.5
Two molecules (c)	−4.5
Two molecules (d)	+5.0

[a] as in (a) with an empty platform between the two adsorbed molecules

To analyze the intermolecular interactions in the adsorbed layer, we used the larger model of the oxidized surface (Fig. 6). As shown in the previous section, the first benzoic acid is likely to bind as in Fig. 11 (i.e. in BB mode on two Ga's close to the protonated oxygen): this adduct was optimized at the ONIOM(PBE1PBE:MSINDO) level, including the DFT layer the organic molecule and the linked Ga atoms, with the 6-31G basis set.

The final geometry is close to that obtained for the small cluster in the previous section, even if in this case the two CO–Ga bonds become quite asymmetric, although maintaining the bridging character. Interestingly, the ring plane is strongly bent towards the surface, indicating that the trench is wide and deep enough to accommodate the molecule with no or very small steric repulsion; on the other hand, a simple inspection of the adduct shows that it is not possible to bind two molecules on opposite platforms. We also optimized an adduct in the BC binding mode on one of the corner Ga atoms (see above): the adsorption energy resulted practically the same as for the BB mode (as already found for the small cluster, see Table 4).

Some possible arrangements for a second adsorbed molecule (in high coverage conditions) are schematically depicted in Fig. 12. Structures (a) and (b) contain two molecules bound in BB mode, with side-to-side arrangements, while (c) and (d) are examples of side-to-face between molecules bound in BB and BC modes; due to the geometry of the adsorbed molecules, strongly bent towards the surface as said above, the face-to-face arrangement cannot be found. The adducts with two benzoic acids were optimized and the adsorption energy was computed at the ONIOM level, with the 6-31G basis set in the DFT layer; as above, the quantum chemical calculation was restricted to the organic moiety and to the Ga atoms involved in the bonds. The resulting energies per adsorbed molecule are reported in Table 4.

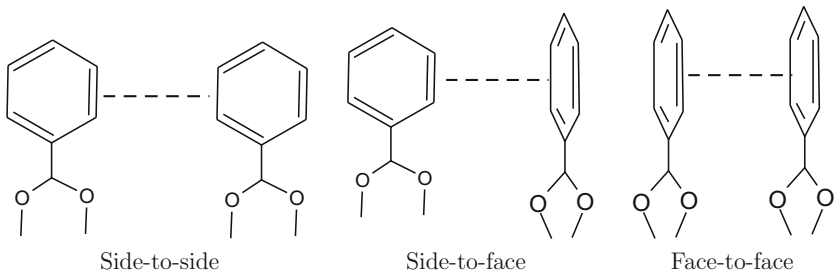

Fig. 9 Different orientations for the benzoic acid dimer

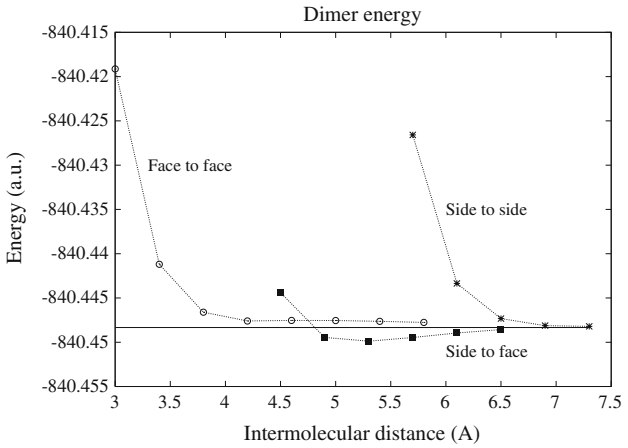

Fig. 10 Benzoic acid dimer energy (a.u.) in different orientations

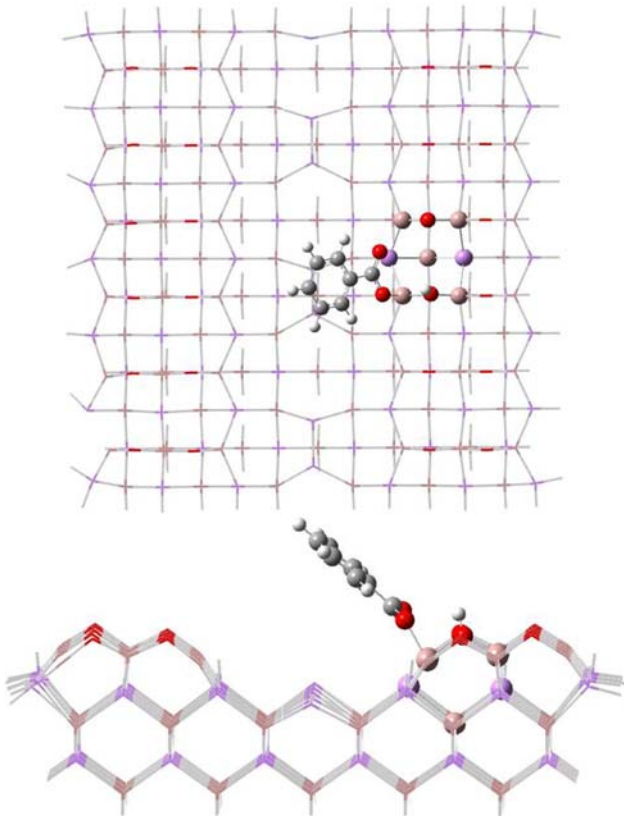

Fig. 11 Benzoic acid adsorbed on the large model of the oxidized surface

In agreement with the results of the dimer energy scan, only the side-to-face arrangement of two molecules on adjacent sites, as in Fig. 12c, shows a stabilizing interaction and yields an adsorption energy per molecule more negative than that of a single benzoic acid. In all the other arrangements the steric interactions prevail, resulting in less favorable adsorption energies. On the basis of these results, the most favored structure for a perfect monolayer of benzoic acid on oxidized GaAs is formed by lines of molecules alternately bound in BB and BC modes on adjacent platforms, as depicted in Fig. 13; only one of such lines can be found in correspondence of each surface trench.

6 Work function changes

As mentioned in Sect. 1, the electrical characteristics of semiconductor or metal junctions can be tuned by adsorbing organic layers on one or both of the contacted surfaces. Being the benzoic acid a prototypical system for carboxylic acids to be adsorbed on semiconductors, a wealth of experimental results are available: in particular, the electron affinity (EA) of GaAs surfaces covered by layers of para-substituted benzoic acid derivatives (BAX, X–Ph–COOH) has been measured by recording the junction current/potential curves under strong illumination. Some models exist, relating the EA change with the electronegativity of the substituents on the benzoic ring (the electron-withdrawing groups inducing higher currents at the same potential): we have shown for a similar case, tartaric acid derivatives on the GaAs (001) surface, that a very effective indicator is the energy of the molecular orbitals most concentrated on the organic moiety with energy close to the HOMO/LUMO levels.

The same correlation was investigated using different BAX, with X = NO_2, OCH_3, H, F, Br, CN, and CF_3,

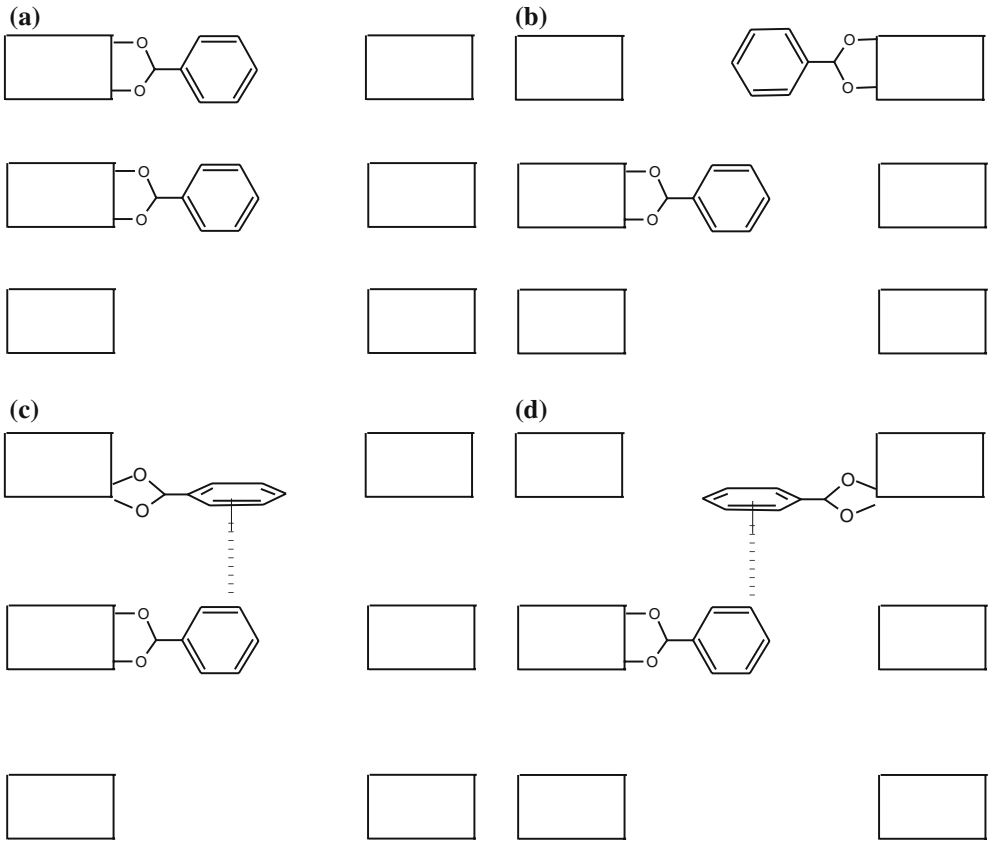

Fig. 12 Schematic picture of two adsorbed molecules

adsorbed on the small model of the oxidized surface $Ga_{20}As_{16}O_4H_{32}$. The adduct structures were optimized at the PBE1PBE/6-31G(d,p) level in the 5,6-BB conformation: the virtual orbital with lowest energy and most concentrated on the benzoic fragment is in all the cases the LUMO+2, depicted in Fig. 14 for X = H. The correlation between this orbital energy and the measured EA changes for derivatized GaAs/metal junctions is illustrated in Fig. 15: a very satisfactory linear relationship is found, confirming the reliability of this indicator to predict the effect of the organic functionalization on the semiconductor electrical properties.

7 Conclusions

The unoxidized and oxidized GaAs (001)-$\beta_2(2 \times 4)$ surfaces have been modeled by clusters of different sizes, at the DFT level and using a hybrid approach combining DFT and semiempical (MSINDO) calculations. The performances of the hybrid approach resulted satisfactory, when compared to the full quantum mechanical calculations. These clusters have been used to investigate the preferred arrangements of adducts formed by one or more benzoic acid molecules adsorbed on the oxidized surface, providing very useful insights into the structure of "perfect" organic layers.

Eight possible arrangements of a single benzoic acid molecule on one of the "platforms" existing on the GaAs surface were examined; both computing their relative energy and comparing their vibrational frequencies to experimental spectra, to select the two most likely structures. Using these structures on a larger cluster (containing several platforms arranged in two parallel lines), we found the only relative orientation displaying a favorable intermolecular interaction, leading to the most likely arrangement for a perfect layer.

Since most applications of devices based on such organic layers on semiconductor surfaces are strongly dependent on the work function of the modified surface, we have followed a procedure earlier applied in a similar case to find a molecular observable related to this macroscopic quantity. In particular, we found that the energy of the adduct lowest empty orbital concentrated on the organic moiety correlates linearly with the measured electron affinity of para-substituted benzoic acids adsorbed on GaAs: this quantity, easily computed on our small model of the organic/inorganic interface,

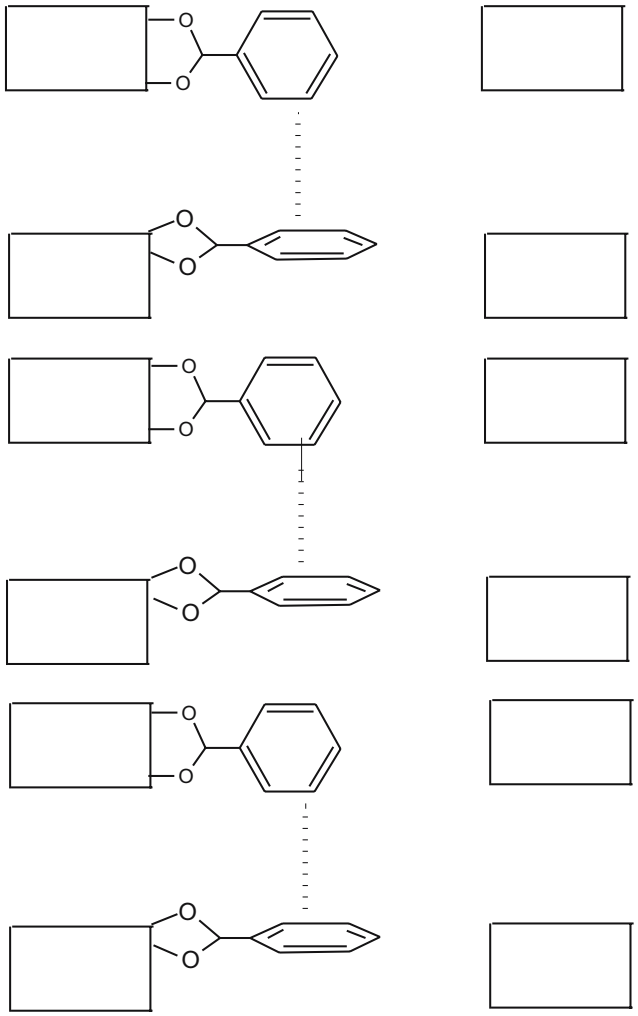

Fig. 13 Minimum energy arrangement for a layer of benzoic acid on oxidized GaAs

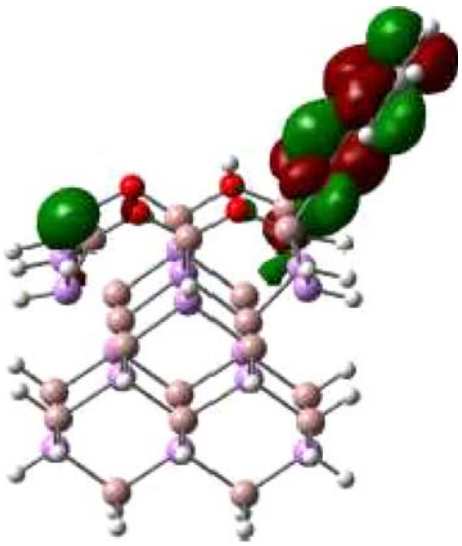

Fig. 14 LUMO+2 molecular orbital for benzoic acid/oxidized cluster adduct

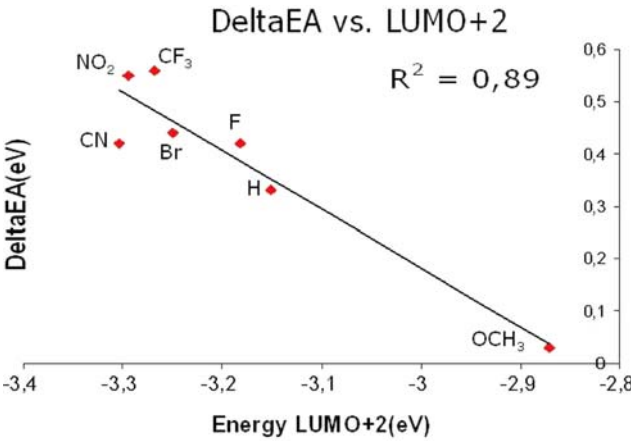

Fig. 15 Linear correlation between the LUMO+2 orbital energy and the observed electron affinity change for derivatized GaAs/metal junctions

can help in design-specific devices, with a predetermined work function.

Acknowledgments The financial support of INSTM (PRISMA project) and MIUR (PRIN project) is gratefully acknowledged.

References

1. Seker F, Meeker K, Kuech TF, Ellis AB (2000) Chem Rev 100:2505
2. Joachim C, Gimzewski JK, Aviram A (2000) Nature 408:541
3. Kronik L, Shapira Y (1999) Surf Sci Rep 37:1
4. Wolkow RA (1999) Ann Rev Phys Chem 50:413
5. Hamers RJ (2001) Nature412:489
6. Ashkenasy G, Cahen D, Cohen R, Shanzer A, Vilan A (2002) Acc Chem Res 35:121
7. Vilan A, Cahen D (2002) Trends in Biotech 20:22
8. Cahen D, Hodes G (2002) Adv Mater 14:789
9. Selzer Y, Cahen D (2001) Adv Mater 13:508
10. Kruger J, Bach U, Gratzel M (2000) Adv Mater 12:447
11. Vilan A, Shanzer A, Cahen D (2000) Nature 404:166
12. Guo Wu D, Ghabboun J, Martin JML, Cahen D (2001) J Phys Chem B 105:12011
13. Guo DW, Ashkenasy G, Shvarts D, Ussyshkin R, Naaman R, Selzer Y, Cahen D (2000) Angew Chem Int Ed Engl 39:4496
14. Selzer Y, Salomon A, Ghabboun J, Cahen D (2002) Angew Chem Int Ed Engl 41:827
15. Campbell IH, Kress JD, Martin RL, Smith DL, Barashkov NN, Ferraris JP (1997) Appl Phys Lett 71:3528
16. Zuppiroli L, Si-Ahmed L, Kamaras K, Nuesch F, Bussac MN, Ades D, Siove A, Moons E, Gratzel M (1999) Eur Phys J B 11:505
17. Visoly-Fisher I, Sitt A, Wahab M, Cahen D (2005) ChemPhysChem 6:277
18. Shvarts Dm, Haran A, Benshafrut R, Cahen D, Naaman R (2002) Chem Phys Lett 354:349
19. Kadyshevitch A, Naaman R, Cohen R, Cahen D, Libman J, Shanzer A (1997) J Phys Chem B 101:4085
20. Vilan A, Ussyshkin R, Gartsman K, Cahen D, Naaman R, Shanzer A (1998) J Phys Chem B 102:3307

21. Shaporenko A, Adlkofer K, Johansson LSO, Ulman A, Grunze M, Tanaka M, Zharnikov M (2004) J Phys Chem B 108:17964
22. Martz J, Zuppiruli L, Nuesch F (2004) Langmuir 20:11428
23. Bastide S, Butruille B, Cahen D, Dutta A, Libman J, Shanzer A, Syn L, Vilan A (1997) J Phys Chem B 101:2678
24. Bonifazi D, Salomon A, Enger O, Diederich F, Cahen D (2002) Adv Mater 14:802
25. Artzi R, Daube SS, Cohen H, Naaman R (2003) Langmuir 19:7392
26. Gartsman K, Cahen D, Kadyshevitch A, Libman J, Moav T, Naaman R, Selzer Y, Umansky A, Vilan A, Chem Phys Lett 283:301
27. Haick H, Ambrico M, Ligonzo T, Cahen D (2004) Adv Mater 16:23
28. Vilan A, Ghabboun J, Cahen D (2003) J Phys Chem B 107:6360
29. Cohen R, Kronik L, Vilan A, Shanzer A, Cahen D (2000) Adv Mater 12:33
30. Lodha S, Janes DB (2004) Appl Phys Lett 85:2809
31. Duke CB (2000) Chem Rev 96:1237
32. Briggs GAD, Fisher AJ (1999) Surface Science Report 33:1
33. Northrup JE, Froyen S (1994) Phys. Rev. B 50:2015
34. Ohno T (1993) Phys Rev Lett 70:631
35. Northrup JE, Froyen S (1993) Phys Rev Lett 71:2276
36. LaBella VP, Yang H, Bullock DW, Thibado PM (1999) Phys Rev Lett 83:2989
37. Schmidt WG, Bechstedt F (1996) Phys Rev B 54:16742
38. Srivastava GP, Jenkins SJ (1996) Phys Rev B 53:12589
39. Xu C, Caffey KP, Burnham JS, Goss SH, Garrison BJ, Winograd N (1992) Phys Rev B 45:6776
40. Cerda J, Palomares FJ, Soria F (1995) Phys Rev Lett 75:665
41. McLean JG, Kruse P, Kummel AC (1999) Surface Science 424:206
42. Passlack M, Abrokwah JK, Yu Z, Droopad R, Overgaard CD, Kawayoski H (2003) Appl Phys Lett 82:1691
43. Yu Z, Overgaard CD, Droopad R, Passlack M, Abrokwah JK (2003) Appl Phys Lett 82:2978
44. Kruse P, McLean JG, Kummel AC (2000) J Chem Phys 113:9224
45. Kruse P, McLean JG, Kummel AC (2000) J Chem Phys 113:9217
46. Yi SI, Kruse P, Hale M, Kummel AC (2001) J Chem Phys 114:3215
47. Sexton JZ, Yi SI, Hale M, Kruse P, Demkov AA, Kummel AC (2003) J Chem Phys 119:9191
48. Gaussian 03, Revision C.02, Frisch MJ, Trucks GW, Schlegel HB, Scuseria GE, Robb MA, Cheeseman JR, Montgomery JA Jr, Vreven T, Kudin KN, Burant JC, Millam JM, Iyengar SS, Tomasi J, Barone V, Mennucci B, Cossi M, Scalmani G, Rega N, Petersson GA, Nakatsuji H, Hada M, Ehara M, Toyota K, Fukuda R, Hasegawa J, Ishida M, Nakajima T, Honda Y, Kitao O, Nakai H, Klene M, Li X, Knox JE, Hratchian HP, Cross JB, Adamo C, Jaramillo J, Gomperts R, Stratmann RE, Yazyev O, Austin AJ, Cammi R, Pomelli C, Ochterski JW, Ayala PY, Morokuma K, Voth GA, Salvador P, Dannenberg JJ, Zakrzewski VG, Dapprich S, Daniels AD, Strain MC, Farkas O, Malick DK, Rabuck AD, Raghavachari K, Foresman JB, Ortiz JV, Cui Q, Baboul AG, Clifford S, Cioslowski J, Stefanov BB, Liu G, Liashenko A, Piskorz P, Komaromi I, Martin RL, Fox DJ, Keith T, Al-Laham MA, Peng CY, Nanayakkara A, Challacombe M, Gill PMW, Johnson B, Chen W, Wong MW, Gonzalez C, Pople JA (2003) Gaussian, Inc., Pittsburgh
49. Perdew JP, Ernzerhof M, Burke K (1996) J Chem Phys 105:9982
50. Adamo C, Barone V (1999) J Chem Phys 110:6158
51. Bruening M, Moons E, Yaron-Marcovich D, Cahen D, Libman J, Shanzer A (1994) J Am Chem Soc 116:2972
52. Cohen R, Bastide S, Cahen D, Libman J, Shanzer A, Rosenwaks Y (1997) Adv Mater 9:746
53. Iozzi MF, Cossi M (2005) J Phys Chem B 109:15383
54. Adamo C, Scuseria GE, Barone V (1999) J Chem Phys 111:2889
55. Adamo C, Barone V (1999) Chem Phys Lett 314:152
56. Adamo C, Barone V (2000) Theor Chem Acta 105:169
57. Hariharan PC, Pople JA (1973) Theor Chim Acta 28:213
58. Dunning TH Jr (1989) J Chem Phys 90:1007
59. Petersson GA, Al-Laham MA (1991) J Chem Phys 94:6081
60. Hay PJ, Wadt WR (1985) J Chem Phys 82:270
61. Wadt WR, Hay PJ (1985) J Chem Phys 82:284
62. Hay PJ, Wadt WR (1985) J Chem Phys 82:299
63. Ahlswede B, Jug K (1999) J Comput Chem 20:563
64. ibidem, page 572
65. Nanda DN, Jug K (1980) Theor Chim Acta 57:95
66. Jug K, Geudtner G, Homann T (2000) J Comput Chem 21:974
67. Bredow T, Geudtner G, Jug K (2001) J Comput Chem 22:861
68. Vreven T, Morokuma K (2000) J Comput Chem 21:1419
69. Vreven T, Morokuma K, Farkas Ö, Schlegel HB, Frisch MJ (2003) J Comput Chem 24:760
70. Krüger T, Sax AF (2002) J Comput Chem 23:371
71. DiLabio GA, Wolkow RA, Johnson ER (2005) J Chem Phys 122:044708
72. DiLabio GA, Hurley MM, Christiansen PA (2000) J Chem Phys 116:9578
73. Antes I, Thiel W (1999) J Phys Chem A 103:9290
74. Sexton JZ, Kummel AC (2003) J Vac Sci Technol B 21:1908
75. Wyckoff RWG (1963) Crystal structures, vol. 1. Wiley, New York
76. Maseras F, Morokuma K (1995) J Comput Chem 16:1170
77. Bakowies D, Thiel W (1996) J Phys Chem 100:10580
78. Humbel S, Sieber S, Morokuma K (1996) J Chem Phys 105:1959
79. Matsubara T, Sieber S, Morokuma K (1996) Int J Quant Chem 60:1101
80. Cui Q, Karplus M (2000) J Phys Chem B 104:3721
81. Li H, Hains AW, Everts JE, Robertson AD, Jensen JH (2002) J Phys Chem B 106:3486